EEET ECOLOGICAL ENGINEERING & ENVIRONMENTAL TECHNOLOGY

Ecological Engineering & Environmental Technology, 2026, 27(8), 104–112
https://doi.org/10.12912/27197050/225129
ISSN 2719–7050, License CC-BY 4.0

Received: 2026.06.17
Accepted: 2026.07.10
Published: 2026.08.01

Cross-platform comparison of red–green–blue vegetation indices on winter wheat: Identifying robust metrics for smartphone-to-satellite calibration

Pavlo Lykhovyd[1*], Mykhailo Retman[1], Dmytro Maksymov[2], Gennadiy Karashchuk[3], Larysa Kucher[4], Oleksandr Kazanok[3]

[1] Department of Reclaimed Lands Use, Institute of Water Problems and Land Reclamation, Vasylkivska 37 Street, Kyiv, Ukraine
[2] Department or Irrigated Agriculture and Decarbonization of Agroecosystems, Institute of Climate-Smart Agriculture of NAAS, Maiatska doroha 24 Street, vil. Khlibodarske, Odesa, Ukraine
[3] Department of Technologies of Production and Processing of Agricultural Products named after Academician V.G. Pelich, Kherson State Agrarian and Economic University, Universitetskyi Avenue 5/2, Kropyvnytskyi, Ukraine
[4] Professor M.K. Shykula Department of Soil Science and Soil Conservation, National University of Life and Environmental Sciences of Ukraine, Heroiv Oborony 15 Street, Kyiv, Ukraine
* Corresponding author's e-mail: pavel.likhovid@gmail.com

ABSTRACT

Timely and precise crop monitoring is essential for precision agriculture, yet spaceborne remote sensing frequently suffers from temporal gaps, cloud cover, and high subscription costs. Consumer-grade smartphone photography offers a low-cost alternative for localized monitoring, though its implementation remains doubtful due to a lack of standardization and calibration. This study evaluated the cross-platform consistency of visible spectrum (RGB) vegetation indices between Sentinel-2A satellite imagery and ground-truth smartphone photography. Field trials were conducted across four winter wheat (*Triticum aestivum* L.) fields, located in the semi-arid zone of Ukraine, systematically capturing crop canopy development across three major phenological stages: tillering, stem elongation, and earing. Six visible-spectrum vegetation indices (ExG, ExGR, GLI, VARI, MGRVI, and CIVE) were evaluated. A comparison of static absolute index values revealed strong cross-platform correlation for ExGR, VARI, MGRVI, and CIVE ($R = 0.74–0.77$). Switching to the daily index change rates analysis dramatically changed cross-platform interoperability. The MGRVI emerged as the only robust metric, achieving a superior dynamic linear correlation ($R = 0.89$) and accounting for 78% of spaceborne variance with an RMSE of 0.014. Other smartphone-derived vegetation indices provided moderate to weak ($R = 0.26–0.66$) correlation with satellite-borne indices, which makes them less suitable for implementation in cross-platform crop monitoring systems. The regression model for smartphone to satellite calibration of MGRVI serves as a precondition of cross-platform interoperability in digital systems of precise crop monitoring.

Keywords: crop monitoring system, environmental monitoring, modified green-red vegetation index, regression modeling, visible spectrum indices.

INTRODUCTION

Precision and timely crop health evaluation through clear, objective indicators remains an important and challenging task in modern agriculture. Recent advancements in remote sensing have simplified and improved for scalable, spatiotemporal agricultural monitoring solutions. Satellite imagery is a source of valuable information about agricultural crops. This information is derived from images captured across different spectral bands using specific mathematical computations, which result in various vegetation indices. Each vegetation index provides unique information about vegetation cover, e.g., water stress, green biomass accumulation, pest outbreaks, etc. There are more than one hundred various vegetation indices developed for different purposes and requiring different spectral bands for calculations, but in general, they can be divided into three major groups, namely: multispectral, hyperspectral, and red-green-blue (RGB or visible spectrum) indices (Xue and Su, 2017).

Multispectral indices require specialized sensors to capture canopy reflectance in bands such as near-infrared (NIR), short-wave infrared (SWIR), and other specific reflectance spectra (Haque et al., 2024). Hyperspectral indices (also called narrow-band indices) use reflectance in red (R) and infrared (IR) spectral bands to detect and characterize the red-edge share of the reflectance spectrum (Colovic et al., 2022). Visible spectrum indices usually operate on raw satellite imagery captured in four channels: red (R), green (G), blue (B), and alpha (A). While the RGB channels are the core of vegetation index evaluation, the alpha channel is responsible for pixel transparency (or cloudiness), and is usually removed in the process of index calculation. Although multispectral and hyperspectral vegetation indices are more specific and usually more accurate in the evaluation of vegetation cover conditions, RGB-based indices are more accessible (as they require fewer sensors) and affordable for most agricultural scientists and practitioners (Fuentes-Peñalillo et al., 2018; Lu et al., 2019). While there are platforms that provide raw and even pre-processed multispectral imagery from different satellites, such as Sentinel-2, Landsat-8, or MODIS, free of charge, they often have limitations in scope, temporal availability, and coverage. High-quality archives of multispectral imagery are usually not free of charge; therefore, they are limited in availability and practical value. In addition, raw multispectral images tell a farmer nothing, while pre-processed imagery with corresponding indices requires a subscription.

Furthermore, RGB-based indices are simpler to retrieve from non-satellite platforms, e.g., UAVs or ground-based camera photography. Even a smartphone camera can capture an image in the visible light spectrum, appropriate for processing and the derivation of RGB-based vegetation indices (İşeri, 2025). Therefore, the cost of crop monitoring using visible spectrum imagery is significantly lower.

However, the problem with RGB-based ground-truth imagery lies in its scalability and calibration with spatial, satellite-retrieved imagery. There is a lack of scientific evidence on the correspondence between smartphone-captured RGB images of crops and satellite-retrieved aerospace photography, which is always subjected to atmospheric corrections and is usually better standardized. In the case of smartphone imagery, its quality can vary significantly depending on the camera module, as well as the environmental conditions when taking the photo (excess or low light, shadows, etc.) (Heinonen and Mattila, 2021). Therefore, the main goal of this study was to establish the relationship between satellite-borne and ground-truth RGB images of winter wheat crops and to find out whether smartphone-based images have any prospects to be used as a replacement for satellite images in the case of having no access to the latter.

MATERIALS AND METHODS

Study area and experimental design

The study was conducted from January to June 2021 and from November 2025 to June 2026 across four agricultural fields cropped with winter wheat (*Triticum aestivum* L.). The fields were located in the Kherson Oblast, Ukraine, within the geographic coordinates of 46.63° N – 46.64° N and 32.53° E – 32.54° E in 2021; 46.72° N – 46.73° N and 32.32° E – 32.34° E in 2025–2026. The region is characterized by a cold steppe semi-arid climate (BSk) with dark-chestnut soils, which are typical for intensive winter wheat cultivation (Peel et al., 2007). All fields followed standard regional agrotechnical practices for winter wheat management, including uniform tillage, fertilization, pest control, and plant care.

Data acquisition

Time-series satellite data were acquired from the European Space Agency's (ESA) Sentinel-2 mission via the OneSoil cloud monitoring platform. Sentinel-2A images were used, which inherently include atmospheric, terrain, and cloud correction. For each field, cloud-free or low-cloud (<10%) scenes matching the ground-truth observation dates and spatial distribution were selected. The digital numbers of the Red (Band 4), Green (Band 3), and Blue (Band 2) channels, possessing a spatial resolution of 10 m, were extracted using a custom script in Wolfram language. Mean pixel values were calculated for each of the 10 fields to represent the overall spaceborne crop canopy state on each target date.

Ground-truth canopy photography was executed systematically alongside satellite imagery collection. Images were captured using a commercial smartphone camera of Sony Xperia XZ2 Premium and iPhone XS Max. To match the nadir viewpoint of the satellite sensor, photos were taken vertically downwards (parallel to the ground surface) at a fixed height of approximately 1.5–1.7 meters above the soil surface level.

To ensure statistical representativeness, 5 to 10 random sub-plots were photographed across a predefined diagonal transit track within each field on every sampling date, and the index values were subsequently averaged per field. Images were saved in uncompressed JPEG format with automatic white balance disabled to minimize internal camera calibration noise.

Temporal synchronization and crop phenology

The monitoring framework was aimed at capturing the critical developmental trajectory of winter wheat. To account for slight discrepancies between precise satellite overpass times and ground-truth field visits, as well as multi-day field sampling campaigns, data collection dates were standardized by converting temporal intervals into their respective midpoints.

The observations were strictly synchronized with three key phenological stages of the crop growth and development, namely:

1. Tillering stage (both during initial growth after sowing, winter dormancy, and spring vegetation renewal): characterized by initial canopy development and low fractional vegetation cover, exposing significant background soil.
2. Stem elongation stage: noted for rapid vertical growth and accelerated biomass accumulation.
3. Earing/Heading stage: distinguished by maximum canopy closure, flag leaf development, and the emergence of spikes. The end of the stage is characterized by vegetative growth cessation and yellowing of leaves and ears.

Visible spectrum vegetation indices calculation

To evaluate the cross-platform consistency of the visible spectrum, six distinct RGB-based vegetation indices were calculated for both the satellite and the averaged smartphone images. Prior to index computation, raw digital numbers (DN) or reflectance values were normalized to relative chromatic coordinates (r, g, b) to reduce illumination intensity fluctuations using Equation 1:

$$r = \frac{R}{R+G+B},\ g = \frac{G}{R+G+B},\ b = \frac{B}{R+G+B} \tag{1}$$

The mathematical equations of the evaluated RGB-indices are structured in Table 1.

An example of the general workflow of the RGB-indices evaluation is presented in Figure 1.

Calculation of daily index dynamics (growth rates)

In addition to comparing the indices from different platforms, growth rates for each index were calculated and compared. To calculate the growth rates, the calculated values of each vegetation index were associated with the temporal scale. The daily rate of index change (Δ) represents the velocity of vegetation canopy development, captured by a certain index, between two consecutive observation dates. It was calculated for each field using Equation 2:

Table 1. Mathematical formulas of the evaluated visible spectrum (RGB) vegetation indices

Index	Full name	Equation	Reference
ExG	Excess green index	2g-r-b	Lucena et al. (2024)
ExGR	Excess green minus excess red index	3g-2.4r-b	Dai et al. (2024)
GLI	Green leaf index	$\frac{2g-r-b}{2g+r+b}$	Dai et al. (2024)
VARI	Visible atmospherically resistant index	$\frac{g-r}{g+r-b}$	Solymosi et al. (2019)
MGRVI	Modified green red vegetation index	$\frac{g^2-r^2}{g^2+r^2}$	Song et al. (2023)
CIVE	Color index of vegetation extraction	0.441r-0.811g+0.385b+18.7874	Zhang et al. (2018)

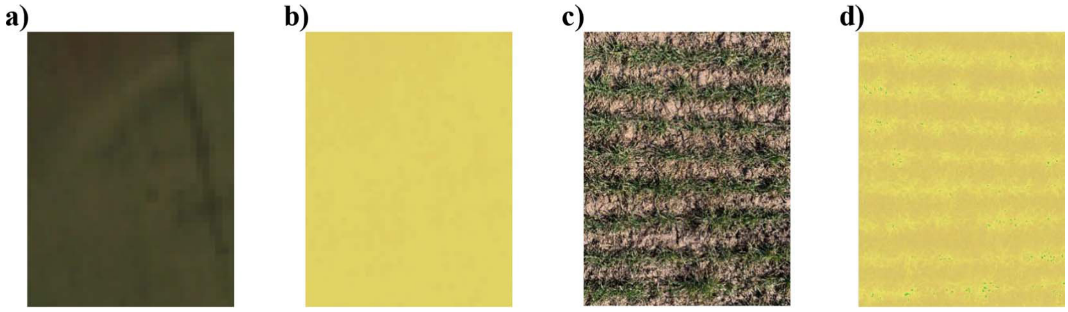

Figure 1. Calculation of visible spectrum (RGB) vegetation indices for winter wheat: (a) satellite image, (b) ExG index map (satellite), (c) smartphone image, (d) ExG index map (smartphone)

$$\Delta = \frac{I_{t2} - I_{t1}}{t_2 - t_1} \quad (2)$$

where: I_{t1} and I_{t2} are the vegetation index values calculated at the corresponding time t_1 and t_2, respectively.

The resulting metric of growth rate was used as an additional metric to establish the interoperability between the satellite and ground-truth smartphone imagery.

Statistical analysis and results evaluation

The strength, direction, and reliability of the cross-platform relationship between smartphone- and satellite-derived indices were quantified using two core statistical parameters. First, Pearson's correlation coefficient (R) was calculated to measure the linear consistency between platforms (Sedgwick, 2012). Second, the coefficient of determination (RSQ) was derived via ordinary least squares (OLS) linear regression analysis to estimate the proportion of variance in the satellite-borne data that can be predictably modeled using ground-based smartphone metrics. In addition, general discrepancy between the smartphone- and satellite-derived indices was estimated by root mean square error (RMSE) and mean absolute percentage error calculation (Chicco et al., 2021). Statistical testing was performed at a significance level of $\alpha = 0.05$. All data processing, image manipulation, statistical modeling, and plot construction were executed using custom Wolfram and Python 3.10 scripts.

RESULTS

Cross-platform comparison of static absolute values of vegetation indices

The average seasonal values of each index, as well as corresponding coefficients of variation (CV), are presented in Table 2. It was established that all the vegetation indices demonstrated higher consistency when derived from satellite imagery, except for GLI. The greatest general inconsistency was recorded for the smartphone-derived ExGR index, while the most stable values were recorded for satellite-derived CIVE. To sum up, the studied indices could be grouped as the extremely inconsistent (VARI, MGRVI, ExGR), somewhat inconsistent (ExG, GLI), and consistent (CIVE) with CV values of higher than 100%, 50–70%, and less than 1%, respectively (Stepniak, 2025).

Table 2. Average seasonal values of visible spectrum (RGB) vegetation indices retrieved from satellite- and smartphone-derived imagery

Metrics	ExG	ExGR	GLI	VARI	MGRVI	CIVE
Satellite-derived						
Average	0.20	0.13	0.14	0.14	0.17	18.75
CV	66.82%	163.00%	65.14%	106.65%	111.25%	0.13%
Smartphone-derived						
Average	0.16	0.04	0.11	0.06	0.08	18.73
CV	62.92%	467.47%	59.81%	189.48%	198.29%	0.24%

Table 3. Pairwise linear correlation-regression analysis of visible spectrum (RGB) vegetation indices retrieved from satellite- and smartphone-derived imagery

Metrics	ExG	ExGR	GLI	VARI	MGRVI	CIVE
R	0.69	0.74	0.68	0.76	0.77	0.74
RSQ	0.48	0.54	0.46	0.58	0.59	0.55
RMSE	0.10	0.16	0.07	0.13	0.15	0.04

Direct comparison of static absolute values of the calculated RGB-indices is required for a general understanding of their mutual correlation and discrepancies. Pairwise Pearson's correlation analysis revealed that four out of six visible spectrum vegetation indices (ExGR, VARI, MGRVI, and CIVE) are strongly related, and the other two (ExG and GLI) are moderately related, respectively (Schober et al., 2018). The strongest correlation was found for MGRVI and VARI (Table 3).

As for the error, the highest was recorded for ExGR values, which was expected, as this index has the intrinsic highest inconsistency. The lowest RMSE was recorded for CIVE, additionally pointing out the stability of this index regardless of the platform. Notably low RMSE was also observed for GLI, which is connected with a moderately strong correlation, testifies to the prospective cross-platform interoperability of this index.

Evaluation of daily change dynamics (growth rates) of vegetation indices

To bypass the absolute baseline differences between spaceborne and smartphone-derived vegetation indices, the analysis was shifted toward the daily growth rate. This approach evaluated how closely both platforms mirror the actual biological acceleration or deceleration of winter wheat development across the stages of tillering, stem elongation, and earing. The statistical evaluation of the daily growth rates revealed a dramatic increase in cross-platform consistency for MGRVI, while other RGB indices demonstrated a reduction in cross-platform interoperability (Table 4).

When tracking daily growth rates rather than static values, MGRVI remained the most robust and superior metric, achieving a strong linear correlation (R = 0.89). The coefficient of determination (R^2 = 0.78) indicates that 78% of the daily growth variance captured by the Sentinel-2A satellite sensor can be precisely explained and modeled by a simple ground-based smartphone photograph. Surprisingly, other indices showed a contrary result – their growth rates correlation decreased dramatically, shifting from strong to moderate or even weak (for GLI) correlation. As for the errors, the smallest RMSE is attributed to CIVE, followed by GLI. The highest RMSE values were established for VARI and MGRVI.

The phenomenal improvement in the statistical metrics of MGRVI when switching to daily growth rates yields a critical scientific insight. This fact confirms a strong coherence between satellite and smartphone imagery, but not for every RGB indicator. Consistent changes in MGRVI values provide a highly synchronized trend direction, serving as an additional marker of strong interoperability between satellite and on-ground crop monitoring platforms. However, other indices should be used cautiously in cross-platform crop monitoring systems.

Regression models for MGRVI within cross-platform crop monitoring systems

Considering the best interoperability performance of MGRVI, linear and quadratic regression models were developed for the prediction of the satellite-borne index values from smartphone imagery (Figure 2).

Table 4. Pairwise linear correlation-regression analysis of visible spectrum (RGB) vegetation indices growth rates based on satellite and smartphone imagery

Metrics	ExG	ExGR	GLI	VARI	MGRVI	CIVE
R	0.32	0.55	0.26	0.66	0.89	0.58
RSQ	0.10	0.30	0.07	0.44	0.78	0.34
RMSE	0.005	0.012	0.003	0.012	0.014	0.002

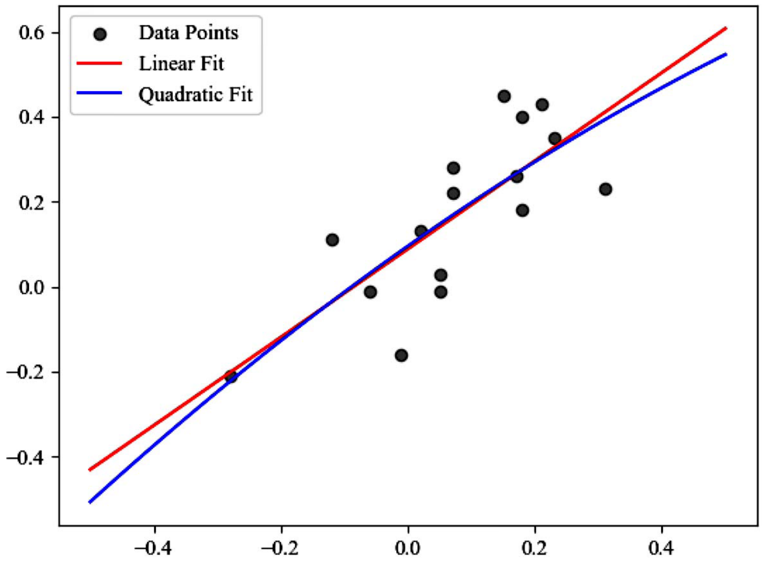

Figure 2. Linear and quadratic models for satellite MGRVI values prediction based on smartphone-derived index values

Table 5. Regression modeling of satellite-borne MGRVI prediction from smartphone-derived index values

Model type	R	RSQ	RMSE	MAPE	Equation
Linear model	0.7667	0.5878	0.1241	1.78%	$y = 1.0374x + 0.0884$
Quadratic model	0.7679	0.5896	0.1244	1.86%	$y = -0.3010x^2 + 1.0522x + 0.0952$

Note: *y* – satellite MGRVI (dependent value); *x* – smartphone MGRVI (independent variable used for prediction).

Statistical metrics for both models are presented in Table 5. It is obvious that both models provided comparable results, with the linear model showing a slightly better prediction accuracy, as indicated by the value of the mean average percentage error (MAPE).

Considering no significant difference was established for the developed models, the linear model shall be preferred because of its generally higher simplicity and lower prediction errors .

DISCUSSION

Timely and precise crop monitoring is essential for precision agriculture. It is also important that crop monitoring is based on a reliable unbiased, and objective source of information, standardized and unified in accordance with certain scientific methodologies. While satellite-based remote sensing data are a cornerstone of modern digital crop monitoring systems, providing objective data on canopy reflectance features, there are numerous limitations to their adoption related to cost, spatial resolution, temporal gaps, and weather-related distortions. Recent advances in portable electronics have enabled the use of consumer-grade smartphone cameras to capture images in the visible light spectrum for calculating various RGB vegetation indices. Using smartphone cameras substantially lowers the price of crop monitoring and also helps to bridge the gaps in remote sensing data when satellite images are not available because of cloud cover or the temporal resolution of the platform. However, the accuracy of smartphone-based assessment of RGB vegetation indices remains questionable. Previous research suggests that it may vary dramatically depending on device camera specifications, internal image-processing algorithms, lighting conditions, and image-capturing geometry (angles and height). Therefore, current research in this field is directed mainly toward determining the reliability and suitability of smartphone-based RGB imagery to supplement or substitute for satellite-based imagery, which is undeniably better standardized and subjected to rigorous initial preprocessing and atmospheric corrections.

Recent studies have revealed that smartphone-captured RGB images show a strong capacity to predict key agronomic parameters of crops, such as above-ground biomass accumulation, dry matter yield, nitrogen content in plant tissues, chlorophyll concentration in leaves, and the fraction of green canopy cover. For example, it was established that visible-spectrum images of red clover crops, captured by a Canon PowerShot ELPH 190 IS from a height of 2.5 m, are suitable for low-cost ExGR index estimation to extract soil background and evaluate canopy development (Rosen et al., 2024). Zolin et al. (2025) studied the relationship between major RGB indices and satellite hyperspectral reflectance indices in wheat and pea crops. Their findings demonstrated that camera-captured RGB indices (especially ExG and VARI) strongly correlate with the normalized difference vegetation index (NDVI) and the photochemical reflectance index (PRI), meaning that visible-spectrum vegetation indices derived from camera-captured images are suitable for assessing pea and wheat growth. Similarly, Nițu et al. (2025) compared smartphone- and UAV-captured RGB indices to satellite-derived NDVI, establishing a strong correlation between green reflectance indices calculated from smartphone images and NDVI values measured by satellite-borne sensors. However, they emphasized that the differences in smartphone cameras introduce systematic discrepancies in imagery quality; therefore, RGB index values from different smartphones cannot be directly compared without previous calibration. Lighting conditions pose an additional threat to smartphone camera performance, with several studies suggesting that controlled acquisition protocols or post-processing corrections are highly recommended (Heinonen and Mattila, 2021). Also, RGB-based indices, especially when derived from regular smartphone cameras, are generally less sensitive than satellite sensors to certain physiological traits of the studied crops, or may underperform in edge cases, e.g., sparse or dense vegetation cover and specific crop architectonics (Ruwanpathirana et al., 2024; Macedo et al., 2025).

As far as the capacities of smartphone cameras differ dramatically across various devices, and it is difficult to systematically adhere to recommended image-capturing techniques in the field conditions, it is hardly arguable that smartphone-derived imagery is rather a supplement than a complete replacement of satellite-borne data. However, our results demonstrated a strong correlation between the smartphone- and satellite-derived MGRVI in winter wheat. Regression modeling additionally confirmed the fact of the interoperability between satellite and smartphone platforms for crop monitoring. Furthermore, the conducted study directly addressed the mentioned above challenges of discrepancies by shifting the analytical focus from static absolute index values to high-frequency temporal dynamics. While recent literature highlights that hardware variances and shifting lighting conditions introduce critical systematic inequalities in absolute RGB metrics, the obtained findings demonstrate that these interferences can be effectively bypassed or at least diminished by calculating daily index change rates. By tracking the actual velocity of winter wheat development across key phenological stages (tillering, stem elongation, and earing), a profound correction in cross-platform interoperability. Most visible spectrum indices fail to deliver an acceptable level of accuracy in cross-platform evaluation, while MGRVI showed even better performance. The developed regression models for MGRVI calibration are easy to understand and simple to implement and integrate into any agronomic decision support system, providing even more room for objective smartphone-based crop monitoring.

CONCLUSIONS

Satellite-derived visible spectrum (RGB) vegetation indices are the cornerstone of modern crop monitoring. Satellite imagery of Sentinel-2A passes through robust atmospheric correction, provides stable capturing parameters, and remains standard in modern remote sensing. Spaceborne RGB indices generally display significantly lower seasonal variation and higher consistency than their smartphone-derived counterparts. Among the evaluated metrics, CIVE proved exceptionally stable across both platforms, maintaining a coefficient of variation below 1.0%. Conversely, ExGR exhibited extreme baseline inconsistency, particularly when captured via near-surface smartphone photography (variation up to 467.47%). While static absolute values of most RGB indices show moderate-to-strong cross-platform correlations (R = 0.68–0.77), shifting the analysis to daily growth rates exposes major functional differences. Most indices undergo severe degradation in cross-platform synchronization when tracking daily dynamics. However, MGRVI stands as a notable exception, with its cross-platform correlation ascending sharply to R = 0.89 in daily change dynamics. This demonstrates that ground-based MGRVI can accurately explain 78% of the daily developmental variance captured from standardized and atmospherically corrected satellite imagery. Satellite-borne MGRVI values can be reliably predicted from low-cost, ground-level smartphone imagery using both linear and quadratic frameworks. Because both models yield highly comparable explanatory power, the linear regression model shall be preferred for integration into digital crop monitoring systems due to its mathematical simplicity and superior predictive precision, evidenced by lower errors. Therefore, MGRVI is the most robust and reliable RGB index for bridging near-surface smartphone photography and satellite telemetry in winter wheat monitoring.

REFERENCES

1. Chicco, D., Warrens, M. J., Jurman, G. (2021). The coefficient of determination R-squared is more informative than SMAPE, MAE, MAPE, MSE and RMSE in regression analysis evaluation. *PeerJ Computer Science, 7*, e623. https://doi.org/10.7717/peerj-cs.623
2. Colovic, M., Yu, K., Todorovic, M., Cantore, V., Hamze, M., Albrizio, R., Stellacci, A. M. (2022). Hyperspectral vegetation indices to assess water and nitrogen status of sweet maize crop. *Agronomy, 12*(9), 2181. https://doi.org/10.3390/agronomy12092181
3. Dai, S., Zhou, J., Ning, X., Xu, J., Wang, H. (2024). Estimation model of wild fractional vegetation cover based on RGB vegetation index and its application. *Open Geosciences, 16*(1), 20220661. https://doi.org/10.1515/geo-2022-0661
4. Fuentes-Peailillo, F., Ortega-Farias, S., Rivera, A., Bardeen, M., Moreno, M. (2018, October). Comparison of vegetation indices acquired from RGB and Multispectral sensors placed on UAV. In 2018 *IEEE International Conference on Automation/XXIII Congress of the Chilean Association of Automatic Control (ICA-ACCA)* (pp. 1–6). IEEE. https://doi.org/10.1109/ICA-ACCA.2018.8609861
5. Haque, M. A., Reza, M. N., Ali, M., Karim, M. R., Ahmed, S., Lee, K. D., Khang, Y. H., Chung, S. O. (2024). Effects of environmental conditions on vegetation indices from multispectral images: A review. *Korean Journal of Remote Sensing, 40*(4), 319–341. https://doi.org/10.7780/kjrs.2024.40.4.1
6. Heinonen, R., Mattila, T. J. (2021). Smartphone-based estimation of green cover depends on the camera used. *Agronomy Journal, 113*(6), 5597–5601. https://doi.org/10.1002/agj2.20752
7. İeri, O. (2025). Usability of smartphone-based RGB vegetation indices for steppe rangeland inventory and monitoring. *Precision Agriculture, 26*(1), 2. https://doi.org/10.1007/s11119-024-10195-0
8. Lu, B., He, Y., Dao, P. D. (2019). Comparing the performance of multispectral and hyperspectral images for estimating vegetation properties. *IEEE Journal of Selected Topics in Applied Earth Observations and Remote Sensing, 12*(6), 1784–1797. https://doi.org/10.1109/JSTARS.2019.2910558
9. Lucena, A., Rendeiro, R., Marques, C. (2024). Vegetation health evaluation using cost-effective aerial reflectance measurements. *EPJ Web of Conferences, 305*, 00005. https://doi.org/10.1051/epjconf/202430500005
10. Macedo, F. L., Nóbrega, H., de Freitas, J. G., Pinheiro de Carvalho, M. A. (2025). Assessment of vegetation indices derived from UAV imagery for weed detection in vineyards. *Remote Sensing, 17*(11), 1899. https://doi.org/10.3390/rs17111899
11. Nițu, A., Florea, C., Ivanovici, M., Racoviteanu, A. (2025). NDVI and beyond: Vegetation indices as features for crop recognition and segmentation in hyperspectral data. *Sensors, 25*(12), 3817. https://doi.org/10.3390/s25123817
12. Peel, M. C., Finlayson, B. L., McMahon, T. A. (2007). Updated world map of the Köppen-Geiger climate classification. *Hydrology and Earth System Sciences, 11*(5), 1633–1644. https://doi.org/10.5194/hess-11-1633-2007
13. Rosen, L., Ewing, P. M., Runck, B. C. (2024). RGB-based indices for estimating cover crop biomass, nitrogen content, and carbon:nitrogen ratio. *Agronomy Journal, 116*, 3070–3080. https://doi.org/10.1002/agj2.21657
14. Ruwanpathirana, P. P., Sakai, K., Jayasinghe, G. Y., Nakandakari, T., Yuge, K., Wijekoon, W. M. C. J., Priyankara, A. C. P., Samaraweera, M. D. S., Madushanka, P. L. A. (2024). Evaluation of sugarcane crop growth monitoring using vegetation indices derived from RGB-based UAV images and machine learning models. *Agronomy, 14*(9), 2059. https://doi.org/10.3390/agronomy14092059
15. Schober, P., Boer, C., Schwarte, L. A. (2018). Correlation coefficients: appropriate use and interpretation. *Anesthesia & Analgesia, 126*(5), 1763–1768. https://doi.org/10.1213/ANE.0000000000002864
16. Sedgwick, P. (2012). Pearson's correlation coefficient. *Bmj, 345*, e4483. https://doi.org/10.1136/bmj.e4483
17. Solymosi, K., Kövér, G., Romvári, R. (2019). The development of vegetation indices: A short overview. *Acta Agraria Kaposváriensis, 23*(1), 75–90. https://doi.org/10.31914/aak.2264
18. Song, Z., Lu, Y., Ding, Z., Sun, D., Jia, Y., Sun, W.

(2023). A new remote sensing desert vegetation detection index. *Remote Sensing, 15*(24), 5742. https://doi.org/10.3390/rs15245742

19. Stepniak, C. (2025). *Coefficient of variation*. In: M. Lovric (Eds.) International Encyclopedia of Statistical Science. Springer, Berlin, Heidelberg. https://doi.org/10.1007/978-3-662-69359-9_117
20. Xue, J., Su, B. (2017). Significant remote sensing vegetation indices: A review of developments and applications. *Journal of Sensors, 2017*(1), 1353691. https://doi.org/10.1155/2017/1353691
21. Zhang, D., Mansaray, L. R., Jin, H., Sun, H., Kuang, Z., Huang, J. (2018). A universal estimation model of fractional vegetation cover for different crops based on time series digital photographs. *Computers and Electronics in Agriculture, 151*, 93–103. https://doi.org/10.1016/j.compag.2018.05.030
22. Zolin, Y., Popova, A., Yudina, L., Grebneva, K., Abasheva, K., Sukhov, V., Sukhova, E. (2025). RGB indices can be used to estimate NDVI, PRI, and Fv/Fm in wheat and pea plants under soil drought and salinization. *Plants, 14*(9), 1284. https://doi.org/10.3390/plants14091284